PHYSICAL REVIEW B **82**, 041404(R) (2010)

Spin-orbit interaction in chiral carbon nanotubes probed in pulsed magnetic fields

S. H. Jhang,[1] M. Marganska,[2] Y. Skourski,[3] D. Preusche,[1] B. Witkamp,[4] M. Grifoni,[2] H. van der Zant,[4] J. Wosnitza,[3] and C. Strunk[1,*]

[1]*Institute of Experimental and Applied Physics, University of Regensburg, 93040 Regensburg, Germany*

[2]*Institute for Theoretical Physics, University of Regensburg, 93040 Regensburg, Germany*

[3]*Dresden High Magnetic Field Laboratory, Forschungszentrum Dresden-Rossendorf, 01314 Dresden, Germany*

[4]*Kavli Institute of Nanoscience, Delft University of Technology, 2628 CJ Delft, The Netherlands*

(Received 17 June 2010; published 15 July 2010)

The magnetoconductance of an open carbon nanotube (CNT)-quantum wire was measured in pulsed magnetic fields. At low temperatures, we find a peculiar split magnetoconductance peak close to the charge-neutrality point. Our analysis of the data reveals that this splitting is intimately connected to the spin-orbit interaction and the tube chirality. Band-structure calculations suggest that the current in the peak regions is highly spin polarized, which calls for application in future CNT-based spintronic devices.

DOI: 10.1103/PhysRevB.82.041404 PACS number(s): 73.63.Fg, 75.47.−m, 73.23.Ad, 85.75.−d

An efficient source of spin-polarized electrons is one of the important building blocks of a future spin-based electronics.[1] Very high degrees of polarization can potentially be achieved by exploiting spin-orbit interaction (SOI).[2,3] Based on the low atomic number $Z=6$ of carbon, the spin-orbit interaction in carbon nanotubes (CNTs) was mostly believed to be very weak, until a recent experiment[4] has demonstrated the effect of spin-orbit interaction in clean CNT quantum dots.

In this Rapid Communication, we present magnetoconductance (MC) data for the complementary situation of an *open* CNT-quantum wire obtained in pulsed magnetic fields. Open quantum wires allow much higher currents (up to microampere) since a whole band participates in the transport rather than the individual levels in the quantum-dot regime. In a parallel magnetic field $B_\parallel$, a small band-gap CNT evolves via a metallic state into a semiconducting one, resulting in a typical peak in the MC.[5,6] In one of our tubes, however, we observed a splitting of this MC peak into two peaks at low temperature. Recording MC traces at different gate voltage V_g shows that the splitting vanishes when moving away from the charge-neutrality point (CNP). A thorough comparison to band-structure calculations reveals that the splitting is explained by the SOI, which becomes strong for small tube diameters. Our analysis predicts a highly spin-polarized current in the peak regions.

The experiments have been performed on devices made of individual CNTs prepared on $Si/SiO_2/Si_3N_4$ substrates. The heavily p-doped Si was used as a backgate and the thickness of the insulating layer was 350 nm. CNTs were grown by means of a chemical vapor deposition method[7] and Pd (50 nm) electrodes were defined on top of the tubes by e-beam lithography. In order to exclude strain effects on the band structure,[8] only straight and long ($\sim$50 μm) CNTs were selected for devices and the distance between two Pd electrodes was $\sim$500 nm. The dc magnetoconductance was studied in pulsed magnetic fields of up to 60 T, applied parallel to the tube axis. The accuracy of the alignment was $\sim\pm 5°$ (see supplementary material for further experimental details).[9]

Figure 1(a) shows the magnetoconductance $G(B_\parallel)$ of a small-band-gap CNT device located near the CNP (diameter $d\sim 1.5$ nm). At 82 K, the conductance G of the tube initially increases to reach a maximum at $B_0=5.9$ T, then it exponentially drops to zero at higher fields due to the Aharonov-Bohm (AB) effect.[5,10] Interestingly, when the device was

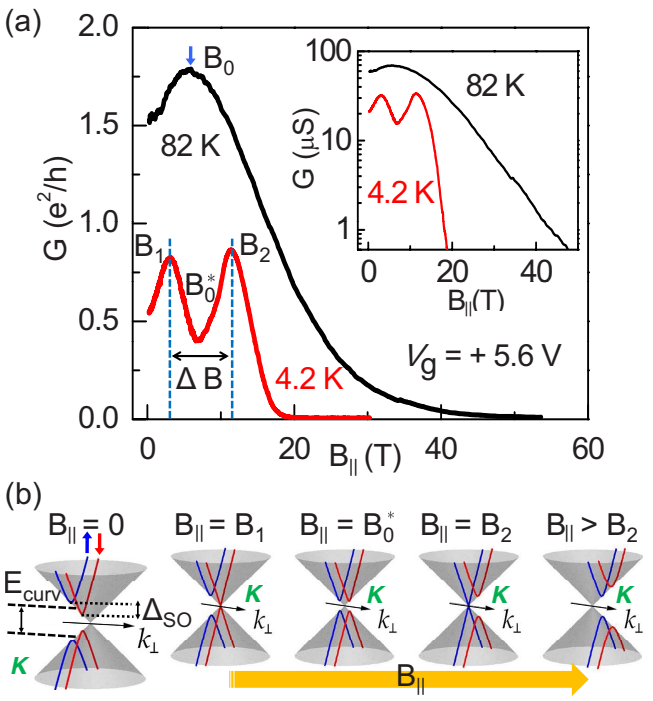

FIG. 1. (Color online) (a) MC of a small-band-gap CNT device near the CNP measured at 82 and 4.2 K. The inset shows the MC in a semilog scale. The observed double peak in $G(B_\parallel)$ defines the characteristic fields B_0^*, B_1, and B_2. (b) One of the Dirac cones near the K points, intersected by lines of allowed $k_\perp$ values for a small-band-gap CNT with SOI. Spin-up and spin-down bands (marked by arrows) display a curvature-induced band gap E_{curv} and are separated by Δ_{SO}, due to the SOI. With increasing $B_\parallel$, spin-split subbands shift due to the AB effect and cross the $K(K')$ point, successively closing the energy gap at B_1 and B_2. For simplicity, the Zeeman term and ε_{SO}, an additional Zeeman-type term induced by the SOI, are neglected. However, B_1 and B_2 are not affected by those terms (see supplementary material) (Ref. 9).

cooled down to 4.2 K, the conductance maximum G_{max} at B_0 was split into two distinct peaks at magnetic fields $B_1 = 3.1$ T and $B_2 = 11.1$ T. We note that these peaks are symmetric with respect to the conductance dip at $B_0^* \approx 7$ T, and $G(B_0^*)$ is similar in magnitude to $G(B_\parallel = 0)$. The key to the explanation of the data lies in the magnetic field dependence of the one-dimensional band structure.

A specific CNT is uniquely labeled by the chiral indices (n,m), which define the chiral angle θ and the quantized values of the transversal wave vector $k_\perp$.[11] The values of $k_\perp$, combined with the graphene dispersion cones, determine the quasi-one-dimensional band structure of the CNTs. A given CNT is metallic if the lines of allowed $k_\perp$ cross the Dirac points K and K'; otherwise it is semiconducting. For nominally metallic CNTs ($n-m=3l$, with l an integer), the dispersion relation $E(k_\parallel)$ near the Dirac points reads[4,12–15]

$$E(k_\parallel) = \pm \hbar v_F \sqrt{k_\parallel^2 + k_\perp^2} + \left(\frac{g}{2}\mu_B B_\parallel + \tau \varepsilon_{SO}\right)\sigma,$$

$$k_\perp = k_{AB} + k_\perp^0 + k_{SO}, \tag{1}$$

where $k_\parallel$ is the wave vector parallel to the tube axis, v_F the Fermi velocity, $\frac{g}{2}\mu_B B_\parallel \sigma$ being the Zeeman term with $\sigma = \pm 1$ for spin parallel/antiparallel to the tube axis, and $\tau = \pm 1$ for the K and K' Dirac points. The transversal wave vector $k_\perp$ contains three distinct contributions, which are discussed below.

The Aharonov-Bohm flux $\phi_{AB} = B_\parallel \pi d^2/4$ results in a shift $k_{AB} = (2/d)(\phi_{AB}/\phi_0)$ of $k_\perp$, where $\phi_0 = h/e$ is the flux quantum. Therefore, one can convert a metallic CNT into a semiconducting one, or vice versa, by tuning the allowed values of $k_\perp$ with a magnetic field parallel to the tube axis.[5,10,16–18]

In addition, curvature[19] affects the allowed values of $k_\perp$ and induces small band gaps in nominally metallic CNTs. The curvature-induced shift[19,20] $k_\perp^0 = -\tau a_0 \cos(3\theta)/(2d)^2$ of the allowed k states results in a band gap $E_{curv} = 2\hbar v_F |k_\perp^0|$ at $B_\parallel = 0$, where a_0 is the C-C bond length.

A second consequence of curvature is a spin-dependent shift,

$$k_{SO} = -\sigma(2/d)(\phi_{SO}/\phi_0), \tag{2}$$

of $k_\perp$ by the spin orbit interaction[4,12–15,21,22] which removes the fourfold spin and K, K' degeneracy in favor of two Kramers doublets corresponding to parallel and antiparallel alignment of orbital and spin magnetic moments. This SOI-induced shift in $k_\perp$ is equivalent to the presence of an AB flux $\phi_{SO} \approx 10^{-3}\phi_0$,[4,12] and produces a spin-orbit energy splitting $\Delta_{SO} = 2\hbar v_F |k_{SO}|$. For a CNT with $d \sim 1$ nm, ϕ_{SO} corresponds to $\simeq 5$ T while ϕ_0 is $\simeq 5000$ T.

In contrast, the term with $\varepsilon_{SO} = -\delta \cos(3\theta)/d$, added to the root in the Eq. (1) (such as the Zeeman term), solely shifts the energy but not $k_\perp$, leading to an asymmetric spin-orbit energy splitting for the hole $(\Delta_{SO} + 2\varepsilon_{SO})$ and the electron band $(\Delta_{SO} - 2\varepsilon_{SO})$ of chiral metallic tubes.[14,15] As ε_{SO} contains the factor $\cos(3\theta)$, it is small for near armchair tubes. The parameter δ ranges from 0.3–0.7 nm meV.[14,15]

The resulting evolution of the band structure in magnetic field is visualized in Fig. 1(b). At zero field, the band gap $E_g^0 = E_{curv} - \Delta_{SO}$ is reduced by the SOI. With the application of $B_\parallel$, the two spin subbands separated by the SOI cross the corner point of the Brillouin zone (either at K or K'), thus explaining two subsequent MC peaks at B_1 and B_2. In between, a conductance dip appears at B_0^* when the spin subbands are located symmetrically around the corner point. If the Zeeman-type terms in Eq. (1) are neglected the energy gap has a local maximum at $k_{AB} = -k_\perp^0$ corresponding to $E_g(B_0^*) \approx \Delta_{SO}$. The distance between the two peaks, $\Delta B = (4/\pi d^2)\Delta\phi_{AB}$, is determined by $\Delta\phi_{AB} = 2\phi_{SO}$ (the factor 2 comes from $\sigma = \pm 1$). For the observed values of $\Delta B = 8$ T and $d = 1.5$ nm, we find

$$\phi_{SO} = \frac{\pi d^2 \Delta B}{8} \approx 1.7 \times 10^{-3}\phi_0. \tag{3}$$

For a conservative confidence interval of ± 0.5 nm for d determined with an atomic force microscope, one obtains $0.76 < 10^3 \phi_{SO}/\phi_0 < 3$ compatible with previous studies.[4,12,21] Equations (1)–(3) result in the energy splitting Δ_{SO} at $B_\parallel = 0$ (assuming $k_\parallel = 0$),

$$\Delta_{SO} = \frac{4\hbar v_F}{d}\frac{\phi_{SO}}{\phi_0} \approx 2.5 \pm 0.8 \text{ meV}. \tag{4}$$

This value corresponds to ~ 30 K and explains the disappearance of the double-peak structure and the single conductance maximum at $B_\parallel = B_0 \simeq B_0^*$ for the 82 K trace of Fig. 1. Because Δ_{SO} is inversely proportional to the diameter, it becomes large for small-diameter tubes.[23]

With further increase in ϕ_{AB}, the energy gap E_g linearly opens again as both orbital subbands gradually move away from the corner points of the Brillouin zone. The exponential decrease in G at high fields [the inset of Fig. 1(a)] is thus explained by charge carriers thermally activated over the magnetic-field-induced band gap, as described by previous authors.[5,24] Since the inset in Fig. 1(a) suggests that the conductance depends exponentially on the band gaps E_g^0 and $E_g(B_0^*)$, they dominate the conductance at $B_\parallel = 0$ and $B_\parallel = B_0^*$. Hence, the approximate equality $G(0) \approx G(B_0^*)$ inferred from Fig. 1(a) suggests the following relation between the two energy scales E_{curv} and Δ_{SO}:

TABLE I. Determination of the chirality from $G(B_\parallel)$ at the charge-neutrality point. ϕ_{SO} was calculated from Eq. (3) with the measured value of $\Delta B = 8$ T and used as input for the evaluation of Δ_{SO} using Eq. (4).

(n,m)	d (nm)	θ (°)	E_{curv} (meV)	B_0, B_0^* (T)	ϕ_{SO} $(10^{-3}\phi_0)$	Δ_{SO} (meV)
(12,9)	1.43	25.3	4.6	7.8	1.54	2.36
(13,10)	1.56	25.7	3.5	5.5	1.84	2.58
(16,10)	1.78	22.4	4.7	6.4	2.39	2.94
(18,9)	1.86	19.1	6.0	7.8	2.63	3.08
(19,10)	2.00	19.8	4.9	5.9	3.02	3.30
(12,3)	1.08	10.9	28.1	63.1	0.88	1.78
(17,2)	1.42	5.5	18.5	31.6	1.51	2.33

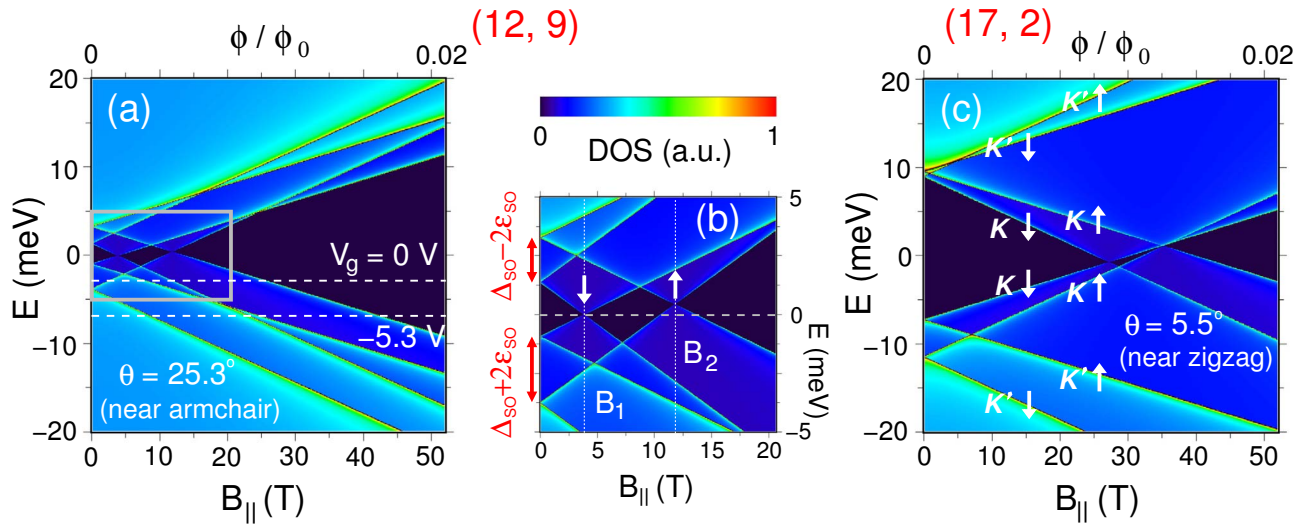

FIG. 2. (Color online) (a) Calculated density of states in a parallel magnetic field for the (12,9) CNT. (b) Zoom into the area bounded by the gray box clearly shows that the band gap is closed at B_1 and B_2 in good agreement with the peak positions observed in Fig. 1(a). White arrows indicate the spin polarization of the bands near the crossing points B_1 and B_2. (c) DOS calculated for the (17,2) CNT. Due to the larger curvature-induced band gap of the (17,2) tube with θ close to 0°, the Zeeman-energy splitting at $B_0(g\mu_B B_0 \approx 3.7$ meV) is larger than the spin-orbit energy splitting ($\Delta_{SO} \approx 2.33$ meV). Hence, the SOI-induced peak splitting is pronounced for the CNTs with chiral angles close to 30°. Orbital (K and K') and spin states (white arrows) are indicated.

$$\frac{E_g^0}{E_g(B_0^*)} = \frac{E_{curv} - \Delta_{SO}}{\Delta_{SO}} \approx 1. \quad (5)$$

We now turn to the discussion of the effect of tube chirality. The strong dependence of B_0 and B_0^* on the chirality can be used to identify the chiral indices of small-band-gap CNTs.[5] Out of 53 small-band-gap CNTs with $d = 1.5 \pm 0.5$ nm, only five tubes [(12,9), (13,10), (16,10), (18,9), and (19,10)] display values of $B_0 \approx 5-8$ T compatible with our data while B_0 can take much larger values for other CNTs, e.g., the (12,3) and (17,2) tubes.

Table I lists values of ϕ_{SO} and Δ_{SO} for these chiralities, calculated from Eqs. (3) and (4) and the observed $\Delta B = 8$ T. The ϕ_{SO} of the (12,9) tube is closest to $\phi_{SO} \approx 10^{-3}\phi_0$, predicted in Ref. 12 and measured in Ref. 4. When we further take into account the condition $E_{curv} \approx 2\Delta_{SO}$ for the CNT measured [Eq. (5)], we realize that the (12,9) and (18,9) tubes satisfy this constraint best.

Taking the (12,9) tube with the chiral angle $\theta = 25.3°$ (close to the armchair configuration) as the most probable candidate, we calculated the density of states (DOS) in a parallel magnetic field. We used the periodic boundary conditions, which are suitable for very long nanotubes. In shorter CNTs the open boundary condition in the axial direction gives rise additionally to edge effects, which are, however, beyond the scope of this work. For comparison, we show the DOS of a (17,2) tube, which has almost the same diameter but a very different chiral angle $\theta = 5.5°$ close to the zigzag configuration.

From Fig. 2, it becomes apparent that in an applied magnetic field the band edges change with four distinct slopes away from the two Kramers doublets both in the electron and hole bands, reflecting the orbital and Zeeman splitting. The DOS calculated for the (12,9) tube explains the evolution of the magnetoconductance very well. The band gap is closed at B_1 by the spin down and subsequently at B_2 by the spin-up subband, in very good agreement with the observed double peaks at the CNP. The calculated energy gaps at zero field and at B_0^* agree with Eqs. (4) and (5). On the other hand, the DOS calculated for the (17,2) CNT predicts a significantly reduced intermediate gap region in Fig. 2(c), in spite of almost the same d and Δ_{SO}, when compared with the (12,9) tube. The (17,2) tube has a much larger curvature-induced gap $E_{curv} \approx 18.5$ meV, resulting in a much higher B_0

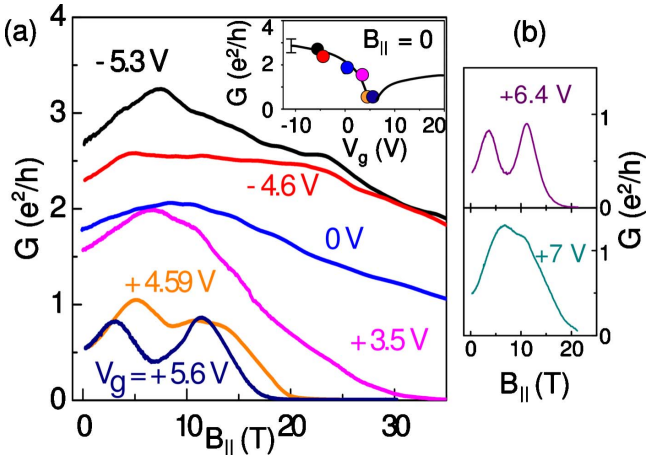

FIG. 3. (Color online) (a) $G(B_\parallel)$ traces at 4.2 K for the hole side of the CNP. As the band gap grows with $B_\parallel$ at high fields, the gate characteristic $G(V_g)$ exhibits the behavior of a p-type CNT field-effect transistor with on-off conductance ratio of several orders of magnitude. The inset shows $G(V_g)$ at $B_\parallel = 0$. The dots correspond to the traces of $G(B_\parallel)$ in main figure. The black solid line in the inset is a fit to experimental points (see error bar) given as a guideline to the eyes. (b) $G(B_\parallel)$ curves for the electron side of the CNP. The double-peak structure is observed only when the Fermi energy is tuned close to the CNP at $V_g \simeq +6$ V.

≈ 31.6 T. Because the spin-orbit gap competes with the Zeeman splitting, the peak splitting in $G(B_\parallel)$ is most pronounced for near armchair tubes with chiral angles close to 30°.

So far, all our discussion focused on the vicinity of the charge-neutrality point. As a crucial test of our analysis, we traced the evolution of the $G(B_\parallel)$ curves for various values of gate voltage. In Fig. 3(a), magnetoconductance traces at 4.2 K are displayed for the hole side of the CNP. Deeply inside the hole band, the conductance exceeds $3e^2/h$, close to the theoretical limit of $4e^2/h$. This shows that our device is in the ballistic regime, where the conductance is determined by the number of available subbands with an average transmission probability of ~ 0.8. At $B_\parallel = 0$, the hole conductance is around $3e^2/h$ and diminishes down to $\sim 0.5e^2/h$ as E_F is tuned toward the CNP ($V_g^* \sim +6$ V). While the magnetoconductance is initially positive at low fields, it becomes negative at high fields ($B_\parallel \gg B_0$) for all gate voltages, indicating the growth of E_g due to the AB effect. At $B_\parallel > 30$ T, the gate characteristic $G(V_g)$ exhibits the behavior of a p-type CNT field-effect transistor with an on-off conductance ratio $>10^3$. The double-peak structure is pronounced only in the vicinity of the CNP ($+5.6 \leq V_g^* \leq +6.4$ V). Two additional $G(B_\parallel)$ curves, presented in Fig. 3(b), show that the two peaks merge again into one as E_F is shifted to the electron side across the CNP.

Approximating the backgate coupling to the Fermi-energy shift as $\Delta E_F \approx 0.7 \times 10^{-3} e \Delta V_g$, the DOS calculation matches the gate voltages in Fig. 3. For instance, the conductance kinks observed at 8 and 24 T for the $G(B_\parallel)$ curve at $V_g = -5.3$ V in Fig. 3(a), may be explained by the subsequent loss of $K'_\downarrow$ subbands at $B \simeq 8$ T and $K'_\uparrow$, $K_\downarrow$ at $\simeq 24$ T in the DOS. However, as the calculation neglects quantum interference effects in the Fabry-Perot regime, such as the AB beating effect,[25] we cannot expect to explain all features of the measured magnetoconductance within our simple model.

In conclusion, we have investigated single-walled carbon nanotubes up to very high magnetic fields. The magnetoconductance of a quasimetallic tube shows a peculiar double peak, which can be explained in terms of spin-split conduction bands, separated by a strong spin-orbit interaction, which exceeds the Zeeman splitting. Our finding may open the path toward the application of CNTs as highly efficient ballistic spin filters.

This research was funded by the Deutsche Forschungsgemeinschaft within GRK 1570 and SFB 689 and partially supported by EuroMagNET under the EU Contract No. 228043.

*christoph.strunk@physik.uni-regensburg.de

[1] I. Žutić, J. Fabian, and S. D. Sarma, Rev. Mod. Phys. **76**, 323 (2004).
[2] Y. K. Kato, R. C. Myers, A. C. Gossard, and D. D. Awschalom, Science **306**, 1910 (2004).
[3] J. Wunderlich, B. Kaestner, J. Sinova, and T. Jungwirth, Phys. Rev. Lett. **94**, 047204 (2005).
[4] F. Kuemmeth, S. Ilani, D. C. Ralph, and P. L. McEuen, Nature (London) **452**, 448 (2008).
[5] G. Fedorov, A. Tselev, D. Jiménez, S. Latil, N. G. Kalugin, P. Barbara, D. Smirnov, and S. Roche, Nano Lett. **7**, 960 (2007).
[6] T. Nakanishi and T. Ando, J. Phys. Soc. Jpn. **74**, 3027 (2005).
[7] J. Kong, H. T. Soh, A. M. Cassell, C. F. Quate, and H. Dai, Nature (London) **395**, 878 (1998).
[8] E. D. Minot, Y. Yaish, V. Sazonova, J.-Y. Park, M. Brink, and P. L. McEuen, Phys. Rev. Lett. **90**, 156401 (2003).
[9] See supplementary material at http://link.aps.org/supplemental/10.1103/PhysRevB.82.041404 for experimental details and effects of the electron-hole asymmetric spin-orbit splitting in energy.
[10] H. Ajiki and T. Ando, J. Phys. Soc. Jpn. **62**, 1255 (1993).
[11] See, e.g., J.-C. Charlier, X. Blase, and S. Roche, Rev. Mod. Phys. **79**, 677 (2007), and references therein.
[12] T. Ando, J. Phys. Soc. Jpn. **69**, 1757 (2000).
[13] D. V. Bulaev, B. Trauzettel, and D. Loss, Phys. Rev. B **77**, 235301 (2008).
[14] W. Izumida, K. Sato, and R. Saito, J. Phys. Soc. Jpn. **78**, 074707 (2009).
[15] J.-S. Jeong and H.-W. Lee, Phys. Rev. B **80**, 075409 (2009).
[16] S. Zaric, G. N. Ostojic, J. Kono, J. Shaver, V. C. Moore, M. S. Strano, R. H. Hauge, R. E. Smalley, and X. Wei, Science **304**, 1129 (2004).
[17] U. C. Coskun, T.-C. Wei, S. Vishveshwara, P. M. Goldbart, and A. Bezryadin, Science **304**, 1132 (2004).
[18] B. Lassagne, J.-P. Cleuziou, S. Nanot, W. Escoffier, R. Avriller, S. Roche, L. Forró, B. Raquet, and J.-M. Broto, Phys. Rev. Lett. **98**, 176802 (2007).
[19] C. L. Kane and E. J. Mele, Phys. Rev. Lett. **78**, 1932 (1997).
[20] A. Kleiner and S. Eggert, Phys. Rev. B **64**, 113402 (2001).
[21] D. Huertas-Hernando, F. Guinea, and A. Brataas, Phys. Rev. B **74**, 155426 (2006).
[22] L. Chico, M. P. Lopez-Sanchó, and M. C. Muñoz, Phys. Rev. B **79**, 235423 (2009).
[23] Therefore, Δ_{SO} is larger for our nanotube, compared to the value observed for the tube ($d \sim 5$ nm) in Ref. 4.
[24] E. D. Minot, Y. Yaish, V. Sazonova, and P. L. McEuen, Nature (London) **428**, 536 (2004).
[25] J. Cao, Q. Wang, M. Rolandi, and H. Dai, Phys. Rev. Lett. **93**, 216803 (2004).

1. Experimental details

The dc magneto-conductance (MC) was studied in pulsed magnetic fields of up to 60 T, applied parallel to the tube axis. The magnetic field pulse resulted from the discharge of a large capacitor bank with a capacitance of 30 mF and a voltage up to 20 kV and lasted typically $\simeq$ 500 ms. To avoid spurious contributions from induction voltages resulting from the magnetic field pulse, relatively high bias voltages ranging from 1-5 mV were required. Combined with nearly ohmic-contact by the Pd electrodes, this suppresses possible effects of Coulomb-blockade. Large bias voltages produce a conductance offset also in gate voltage ranges, where a gap is present, without affecting the peak position in magnetic field. The current was measured using a low noise current amplifier (DL Instruments, model 1211) connected to a scopecorder (Yokogawa, model DL750) which sampled the current for every 100 ns. Overall, about 20 devices were tested in high magnetic field. In many of the devices, the magneto-conductance behavior was rather complex because the disorder smoothed the AB effect on the band structure, and the weak localization and the universal conductance fluctuations started to play a role. Only in 3 devices, the AB effect on the band structure was clearly observed. For these devices, the conductance changes more than 1,000 times as the band gap of the tube is modulated with a magnetic field. One device is reported in the present manuscript, a second had a problem with a gate, and could not be investigated extensively. The third device was a wide-band semiconducting tube of 8 nm diameter, which is not expected to show the important spin-orbit effects.

2. Aharonov-Bohm (AB) effect on a small band-gap CNT without spin-orbit interaction

The figure on the right shows Dirac-like dispersion cones near the K and K' points, intersected by lines of allowed $k_\perp$ values for a small band-gap CNT. The misalignment between lines and K-points ($\pm k_\perp^0$) corresponds to the curvature-induced band gap of the tube. With the application of $B_\parallel$, the lines shift by $k_{\rm AB}$ due to the Aharonov-Bohm (AB) effect, leading at B_0 to the closure of the small gap for one of the K-points when $k_{\rm AB} = -k_\perp^0$. The energy gap then linearly grows again with further increase of $B_\parallel$ as both orbital sub-bands move away from the K-points. Therefore, a small band-gap CNT evolves via a metallic state into a semiconducting one, resulting in a typical peak in the MC. This model can explain the MC data at 82 K shown in Fig. 1a, but not at 4.2 K.

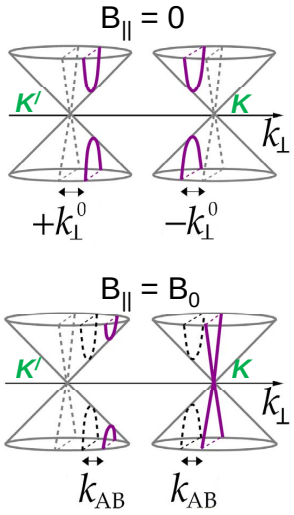

3. Effects of the electron-hole asymmetric spin-orbit splitting in energy

In this paper, we measure the strength of the spin-orbit coupling in transversal $k_\perp$ direction by checking the distance ΔB between two split magneto-conductance (MC) peaks. Reflecting recent theoretical works which explain the asymmetry in the spin-orbit energy splitting for electron and hole bands observed in Ref. 4, $\varepsilon_{\rm SO}$, the term responsible for the asymmetry, is introduced in the dispersion relation of Eq. (1). However, here we show that ΔB is not affected by the electron-hole asymmetry in the energy splitting.

The Eq. (1) of the paper is

$$\begin{aligned} E(k_\parallel) &= \pm\hbar v_F \sqrt{k_\parallel^2 + k_\perp^2} + (\frac{g}{2}\mu_B B_\parallel + \tau\,\varepsilon_{\rm SO})\sigma, \\ \text{with} \quad k_\perp &= k_{\rm AB} + k_\perp^0 + k_{\rm SO}. \end{aligned}$$

Here $\tau = \pm 1$ for K (+) and K' (-) points, and $\sigma = \pm 1$ for spin parallel/antiparallel to the tube axis. Note that there are two different spin-orbit contributions, $k_{\rm SO}$ and $\varepsilon_{\rm SO}$, in the equation.

$$\begin{aligned} k_{\rm SO} &= -\sigma\,\frac{2}{d}\,\frac{\phi_{\rm SO}}{\phi_0}, \\ \varepsilon_{\rm SO} &= -\delta\,\frac{\cos(3\theta)}{d} \quad [\,\delta = -\alpha\,V_{\rm SO}, \quad \text{where } V_{\rm SO} \approx 15 \text{ meV}, \alpha = -0.45\text{Å} \quad \text{(Ref. 14)}\,]. \end{aligned}$$

As shown in Figure S1, the term $k_{\rm SO}$, included under the root in the equation, gives a spin-dependent shift in the quantization condition for $k_\perp$ (such as the Aharonov-Bohm (AB) phase). Hence, $k_{\rm SO}$ can be regarded as an effective AB flux due to the spin-orbit interaction (SOI). On the other hand, $\varepsilon_{\rm SO}$, added to the root in the equation (such as the Zeeman term), gives a spin-dependent energy shift, i.e. $\varepsilon_{\rm SO}$ is an effective Zeeman term owing to the SOI. The calculated density of states (DOS) for the (12,9) tube, taking into account both terms, is displayed in Figure S2, together with the result without the term $\varepsilon_{\rm SO}$ (dashed red lines). The MC peaks appear exactly at the same B_1 and B_2 regardless of $\varepsilon_{\rm SO}$, but with a small shift in the energy due to the effective Zeeman term $\varepsilon_{\rm SO}$.

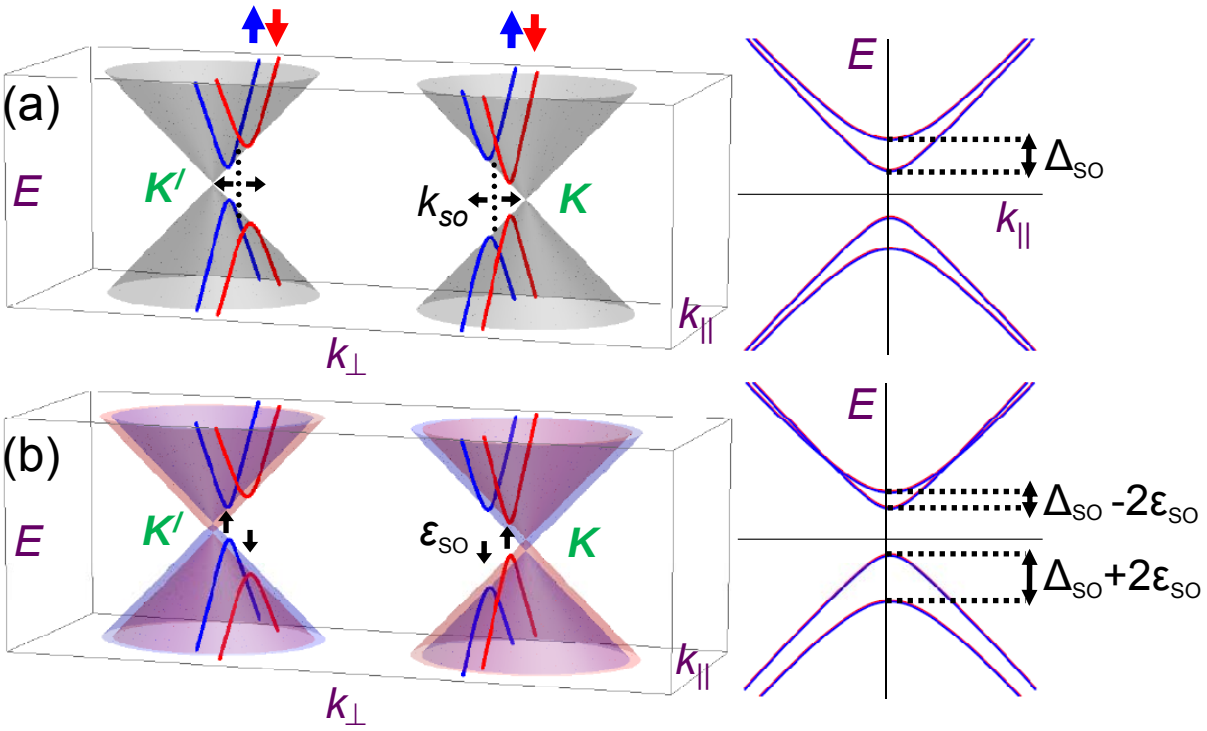

FIG. S1: (a) Dirac cones near the K-points, intersected by lines of allowed $k_\perp$ values for a small-bandgap nanotube with the spin-orbit contribution in $k_\perp$ direction, and the corresponding energy band (on the right). Spin-up (blue) and spin-down (red) states are shifted by $k_{\rm SO} = \mp(2/d)(\phi_{\rm SO}/\phi_0)$, respectively, due to the spin-orbit interaction. The shift by $k_{\rm SO}$ in transversal $k_\perp$ induces the splitting in energy $\Delta_{\rm SO}$ both for the hole and the electron bands. (b) Taking into account the term $\varepsilon_{\rm SO}$, the spin-up (blue) and spin-down (red) states are additionally shifted in energy by $\pm\tau\,\varepsilon_{\rm SO}$, respectively. Here $\tau = \pm 1$ for K (+) and K' (-). Including both contributions, the energy splitting of chiral metallic tubes becomes $\Delta_{\rm SO} + 2\varepsilon_{\rm SO}$ for the hole band, and $\Delta_{\rm SO} - 2\varepsilon_{\rm SO}$ for the electron band. As $\varepsilon_{\rm SO}$ contains the factor $\cos(3\theta)$, the term is small for near armchair tubes.

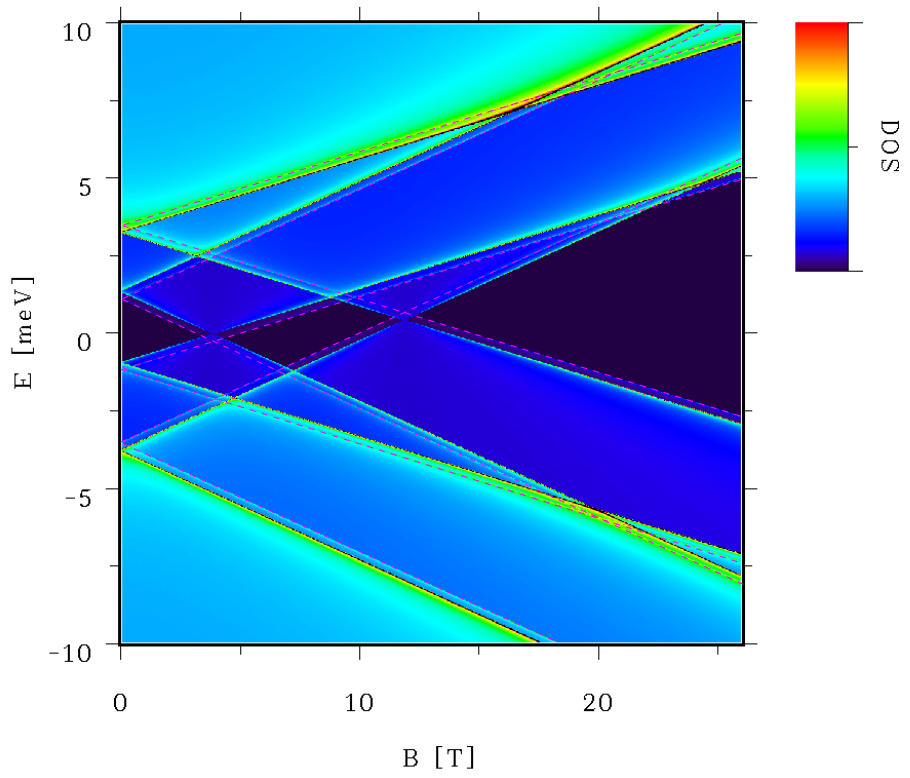

FIG. S2: Calculated density of states (DOS) for the (12,9) tube including both spin-orbit contributions, $k_{\rm SO}$ and $\varepsilon_{\rm SO}$. The dashed red lines indicate the result without $\varepsilon_{\rm SO}$ for comparison. Magneto-conductance peaks are expected exactly at the same B_1 and B_2.